Korean Journal of Remote Sensing, Vol.36, No.4, 2020, pp.609~626
https://doi.org/10.7780/kjrs.2020.36.4.9

ISSN 1225-6161 (Print)
ISSN 2287-9307 (Online)

Review

Spatial Downscaling of MODIS Land Surface Temperature: Recent Research Trends, Challenges, and Future Directions

Cheolhee Yoo [1)*] · **Jungho Im** [2)*†] · **Sumin Park** [1)] · **Dongjin Cho** [1)]

Abstract: Satellite-based land surface temperature (LST) has been used as one of the major parameters in various climate and environmental models. Especially, Moderate Resolution Imaging Spectroradiometer (MODIS) LST is the most widely used satellite-based LST product due to its spatiotemporal coverage (1 km spatial and sub-daily temporal resolutions) and longevity (> 20 years). However, there is an increasing demand for LST products with finer spatial resolution (e.g., 10-250 m) over regions such as urban areas. Therefore, various methods have been proposed to produce high-resolution MODIS-like LST less than 250 m (e.g., 100 m). The purpose of this review is to provide a comprehensive overview of recent research trends and challenges for the downscaling of MODIS LST. Based on the recent literature survey for the past decade, the downscaling techniques classified into three groups—kernel-driven, fusion-based, and the combination of kernel-driven and fusion-based methods—were reviewed with their pros and cons. Then, five open issues and challenges were discussed: uncertainty in LST retrievals, low thermal contrast, the nonlinearity of LST temporal change, cloud contamination, and model generalization. Future research directions of LST downscaling were finally provided.

Key Words: land surface temperature, spatial downscaling, kernel-driven, machine learning, data fusion, MODIS

1. Introduction

Land surface temperature (LST), the skin temperature of the Earth surface, is one of the major variables of climate systems, and has been used as a key parameter in modeling surface energy balance (Bateni *et al*., 2013; Alkhaier *et al*., 2012; Hain and Anderson, 2017). LST interacts with other factors such as soil moisture, air temperature, and evapotranspiration (Srivastava *et al*., 2013; Yoo *et al*., 2018; Meng *et al*., 2009). In particular, LST has been widely used in investigating various socio-environmental problems such as heatwave,

Received August 15, 2020; Revised August 19, 2020; Accepted August 21, 2020; Published online August 25, 2020

[1)] Combined MS/PhD Student, School of Urban and Environmental Engineering, Ulsan National Institute of Science and Technology
[2)] Professor, School of Urban and Environmental Engineering, Ulsan National Institute of Science and Technology

[†] Corresponding Author: Jungho Im (ersgis@unist.ac.kr)

[*] These authors contributed equally to this work.

drought, air quality, and urban heat island effect (Albright *et al*., 2011; Park *et al*., 2020; Yoo *et al*., 2019; Ziaul and Pal, 2018).

LST has relatively large variation in both spatial and temporal domains due to the complicated characteristics of environmental factors such as vegetation coverage, topography, soil texture, and land cover patterns, which are closely related to LST. Although *in-situ* ground measurements provide accurate surface temperature at a location, they do not provide spatially continuous LST information over vast areas. Satellite remote sensing has been a good alternative to spatiotemporal LST delineation from regional to global scale. Thermal infrared (TIR) sensors are a major source for producing satellite-based LSTs under clear sky conditions. Widely used polar orbiting TIR sensors include Moderate Resolution Imaging Spectroradiometer (MODIS; Wan, 1999), The visible infrared imaging radiometer suite (VIIRS; Hulley *et al*., 2016a), advanced spaceborne thermal emission and reflection radiometer (ASTER; Abrams *et al*., 2002), Landsat-8 Thermal Infrared Sensor (TIRS; USGS, 2016). LSTs can be also obtained from geostationary satellite sensors with high temporal resolution such as spinning enhanced visible and infrared imager (SEVIRI; Atitar *et al*., 2008), GeoKompsat-2A (GK-2A, NMSC: GK-2A AMI Algorithm Theoretical Basis Document) Advanced Meteorological Imager (AMI), Himawari-8 Advanced Himawari Imager (AHI; Yamamoto *et al*., 2018), and Geostationary Operational Environmental Satellites (GOES)-16 Advanced Baseline Imager (ABI; Yu *et al*., 2010), which can be used to look into the diurnal cycle of LST. To minimize the cloud contamination when using TIR sensors, previous studies have produced LSTs from brightness temperature collected by passive microwave satellite sensors such as the advanced microwave Scanning radiometer-earth observing system (AMSR-E) and advanced microwave scanning radiometer 2 (AMSR2) (Yoo *et al*., 2020; Duan *et al*., 2020).

Among various satellite-based LSTs, MODIS LST is the most widely used LST product in modeling atmosphere, ocean and land processes on the Earth thanks to its spatiotemporal coverage and longevity (> 20 years). MODIS sensors onboard Terra and Aqua satellites collect data providing LST four times a day (local solar times of 10:30 am and 10:30 pm for Terra, and 1:30 am and 1:30 pm for Aqua) at 1 km spatial resolution. MODIS LST is generated based on the generalized split-window algorithm and is provided as global grid data at multiple time scales (i.e., daily, eight-day, and monthly LSTs). One of the drawbacks of MODIS LST is its relatively coarse spatial resolution (i.e., 1 km). With the increasing demand of satellite-derived products in various areas under changing climate conditions, information of detailed thermal environment on the Earth surface at high resolution (e.g., 10-100 m) is required (Hulley *et al*., 2019). In particular, the use of 1 km MODIS LST over urban areas showing very heterogeneous thermal surface characteristics is limited (Yoo *et al*., 2020).

There are several satellite sensors that globally provide fine resolution (~100 m) LSTs, such as Landsat series and ASTER. However, their temporal resolutions relatively low around 16 days, limiting investigation of temporal variation of LSTs. To solve the trade-off between the spatial and temporal resolution of remote sensing-derived products such as LST, many studies have provided spatiotemporal downscaling methods using multi-sensor data. In particular, due to the complexity of thermal landscapes, many factors should be considered when performing thermal downscaling, which is also known as thermal sharpening or disaggregating (Weng *et al*., 2014). The thermal downscaling of 1 km MODIS LST through a multitude of techniques can generate high spatial resolution daily LST products typically ranging from 100 m to 250 m. In addition, the downscaled LSTs (hereafter DLSTs) have been actively used in various areas such as monitoring thermal processes (i.e., urban heat island) or estimating other environmental products (i.e.,

evapotranspiration) (Yoo *et al*., 2017; Liu *et al*., 2019).

Many approaches for thermal downscaling of MODIS LSTs have been developed during the past decade showing varied performance and efficiency. Each approach has its own merits and limitations, and there are still key challenges that should be carefully addressed in future research. The aim of this paper is to provide a comprehensive review on recent thermal downscaling methods focusing on MODIS LSTs. This review first groups the thermal downscaling methods for the past decade into three categories. Detailed discussion for each group in terms of its advantages and limitations follows. Then, challenges and future research direction are highlighted. The present review paper can assist to improve the applicability of DLSTs in a variety of research fields such as meteorology, urban climatology and hydrology.

2. Downscaling Methods

We categorized MODIS LST downscaling methods in three types: Kernel-driven, image fusion-based, and the combination of both (Fig. 1).

1) Kernel-driven methods

The kernel-driven method is the most frequently used thermal downscaling approach in recent years. The kernel-driven method spatially aggregates high resolution input variables matching the MODIS LST scale, then models the relationship between LSTs rtand the upscaled input variables. Finally, the method applies the developed model to the original high resolution input variables, called kernels, to produce high resolution LSTs (Fig. 2). In addition, most kernel-driven method applied a residual correction process originally suggested by Kustas *et al*. (2003). This process generally uses the following steps: 1) aggregating the simulated high resolution LST (LST_{high}) to the original MODIS LST scale, 2) subtracting the aggregated LST_{high} (LST_{ag}) from original MODIS LST (called residuals; Δ), 3) resampling the residuals to LST_{high} scale and adding these residuals to the LST_{high} for generating MODIS DLST (equations (1) and (2)).

$$\Delta = MODIS\ LST - LST_{ag} \quad (1)$$

$$MODIS\ DLST = LST_{high} + \Delta \quad (2)$$

The spatial resolution of DLST is determined by the resolution of the kernels. There are many factors that affect the performance of the kernel-driven approach, including types of kernels and modeling techniques. MODIS spectral reflectance data at 250 m (i.e., red and near-infrared (NIR) bands) can be used as kernels for thermal downscaling of MODIS LSTs produced at the same time. In particular, normalized difference vegetation index (NDVI) is calculated using the red and

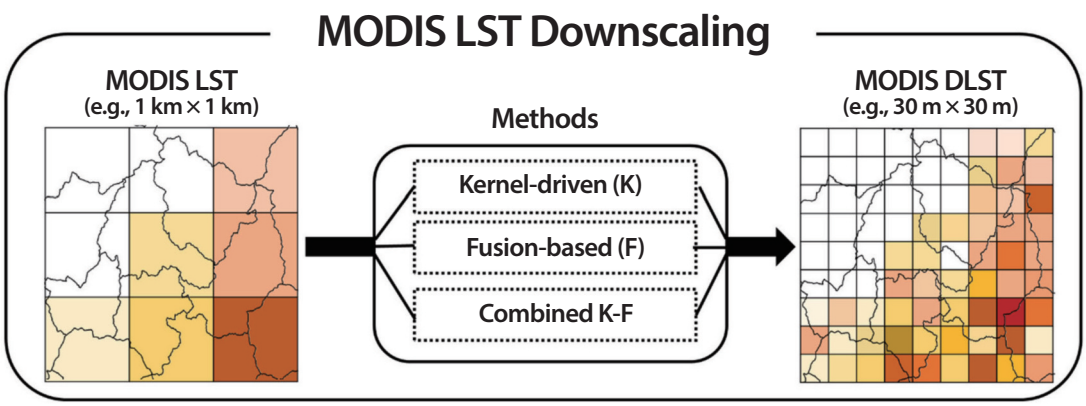

Fig. 1. Three types of MODIS LST downscaling approaches.

NIR bands. Since there is a linear relationship between NDVI and LST, NDVI has been used as a useful kernel for thermal downscaling. This downscaling approach using NDVI is the basic kernel-driven method, which is called the thermal sharpening algorithm (TsHARP).

Mukherjee *et al*. (2014) compared various kernel-driven models using NDVI: TsHARP, polynomial regression model (DisTrad), Last median square regression (LMSDS), and Pace regression (PRDS). They reported that LMSDS resulted in the lowest root-mean-square-error (RMSE) of 1.43K when using Landsat LST as reference data. Qiu *et al*. (2018) reported that enhanced vegetation index (EVI) was more effective than NDVI as a kernel in DisTrad over areas with a high vegetation cover rate such as forest. Another widely used kernel along with vegetation indices is digital elevation models (DEM) such as Shuttle Radar Topography Mission (SRTM) or ASTER-derived DEM. Maeda (2014) adopted multivariate regression using NDVI and DEM as kernels to generate 250 m monthly MODIS DLST. The studies mentioned above assumed that there are linear relationships between LST and kernels such as NDVI and DEM, and thus the proposed methods would not work well over areas where the relationships were not linear.

In order to downscale MODIS LST to less than 250 m resolution (e.g., 100 m), higher spatial resolution data than MODIS reflectance (250 m) should be used as kernels in a model. While Landsat and ASTER satellite data have been used as high resolution kernels in thermal downscaling of MODIS LST, they have relatively low temporal resolution (i.e., 16 days). Many studies assumed that there is little difference in reflectance collected in close dates and used Landsat or ASTER data collected in near-anniversary dates with MODIS LST as kernels. Bonafoni (2016) calculated NDVI and normalized difference building index (NDBI) from Landsat data and used them as kernels to generate 120 m MODIS DLST using ridge regression. Similarly, Duan and Li (2016) adopted geographically weighted regression using ASTER NDVI and SRTM DEM as kernels to downscale MODIS LST to 90 m.

In particular, when study sites are urban areas, kernels highlighting built-up area can be effective in

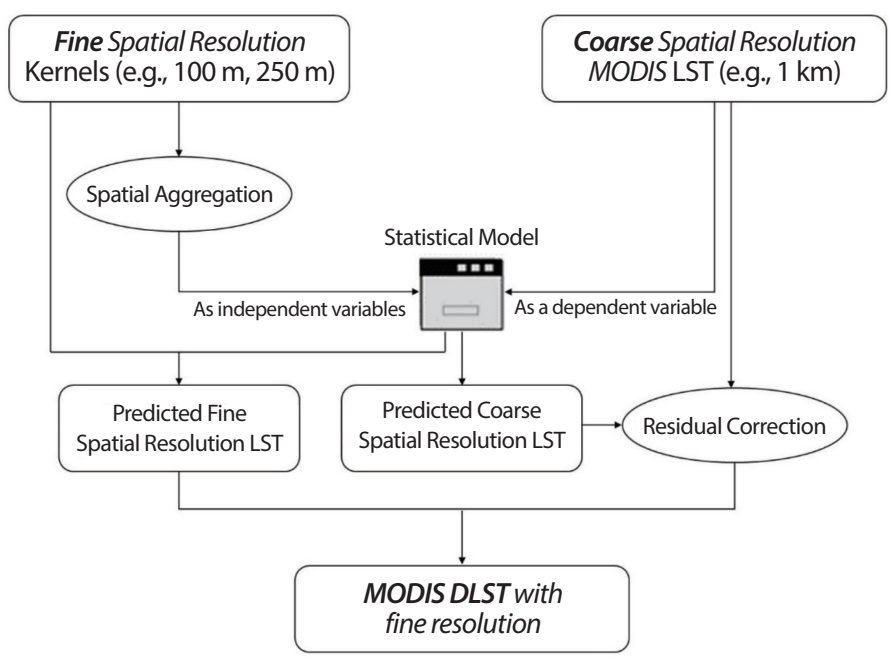

Fig. 2. Flowchart of a typical kernel-driven method for LST downscaling.

MODIS LST downscaling. For example, Sattari *et al*. (2018) improved the performance of TsHARP by replacing MODIS NDVI with the ASTER-derived impervious surface index over the city of Kuala Lumpur, Malaysia. NDBI has been also useful as a kernel in urban areas. Wang *et al*. (2020b) used Landsat 8-derived NDBI and SRTM DEM as kernels in geographically weighted autoregressive regression (GWAR) over Beijing and Lanzhou, China, resulting in better performance (RMSEs of 1.37K for Beijing and 1.76K for Lanzhou) than TsHARP (RMSEs of 2.53K for Beijing and 3.46K for Lanzhou). Peng *et al*. (2019) downscaled MODIS LST to 100 m based on geographically and temporally weighted regression model (GTWR) using Landsat NDBI and SRTM DEM as kernels.

Recently, machine learning approaches have been used to model the non-linearity between the kernels and LST (Bartkowiak *et al*., 2019; Liu *et al*., 2020a; Yang *et al*., 2017; Ebrahimy and Azadbakht, 2019). Bartkowiak *et al*. (2019) adopted random forest (RF) to generate 250 m MODIS DLST using NDVI and DEM. Liu *et al*. (2020a) tested three kernels—NDVI, temperature vegetation dryness index (TVDI), and fractional vegetation coverage (FVC)—using RF and concluded that TVDI was effective in MODIS LST downscaling over agricultural regions where soil moisture plays an important role. Other satellite-derived indices representing the characteristics of vegetation, water, soil moisture, impervious surface, and desert (i.e., soil-adjusted vegetation index (SAVI), NDBI, normalized difference dust index (NDDI), and modified normalized difference water index (MNDWI)) have been also used as kernels in RF to generate 250 m MODIS DLST (Yang *et al*., 2017). In addition to reflectance-based indices, various topographic parameters (i.e., elevation, slope, and aspect), solar incidence, solar radiation, and sky view factor have been used as kernels in RF models (Hutengs and Vohland, 2016; Yoo *et al*., 2017). Ebrahimy and Azadbakht (2019) determined 11 kernels such as NDVI, SAVI, DEM, and sky view factor over Teheran, Iran through feature selection, and used them in three machine learning approaches—RF, support vector regression (SVR), and extreme learning method (ELM)—to produce 250 m MODIS DLST. They reported that all three models resulted in higher accuracy (averaged RMSE of 2.5K) than TsHARP (RMSE of 3.02K) and ELM was more time efficient than the other two machine learning models.

Machine learning approaches also have been actively used to downscale MODIS LST to the 100 m resolution level. For example, Agathangelidis and Cartalis (2019) used a total of 18 kernels including NDVI, EVI, SAVI, and DEM in RF machine learning to produce 100 m MODIS DLST. Pan *et al*. (2018) generated 90 m MODIS DLST using Landsat-derived NDSI, SAVI, NDWI, and NDBI as kernels in RF. Among machine learning approaches, RF has proved to be more effective than TsHARP to produce 100 m MODIS DLST (Wang *et al*., 2020b; Wu and Li, 2019). Li *et al*. (2019) compared three machine learning approaches—RF, Support Vector Machine (SVM), Artificial Neural Network (ANN)—to produce 90 m MODIS DLST and reported that RF resulted in the best performance while SVM tended to show smoothing effect in the LST distribution. More recently, studies have been conducted to downscale MODIS LST to higher spatial resolution than 90 m. For instance, Sánchez *et al*. (2020) used 10 m Sentinel-2 NDVI to produce 10 m MODIS DLST based on TsHARP over Barrax in Spain with cropland as a dominant land cover.

2) Fusion-based methods

Fusion-based methods determine the relationship between the image pairs (known) of fine resolution LST and coarse resolution LST, and downscale coarse resolution LST (e.g., MODIS LST) when fine resolution LST is not available. Compared to the kernel-driven methods that depend on kernel acquisition time, the fusion-based methods are less restrictive in selecting

Table 1. Description of acronym of fusion-based methods mentioned in this paper

Acronym	Description	Representative Reference
STARFM	Spatial and temporal adaptive reflectance fusion model	Gao *et al*. (2006), Liu and Weng (2018), Wu *et al.* (2015)
SADFAT	Spatio-temporal Adaptive Data Fusion Algorithm for Temperature mapping	Weng *et al*. (2014)
ESTARFM	Enhanced STARFM	Zhu *et al*. (2010), Wu *et al*. (2015), Yang *et al*. (2016), Li *et al*. (2016), Liu *et al*. (2020)
STTFN	Spatiotemporal temperature fusion network	Yin *et al*. (2020)

the target date of DLST in that they directly model two LST images instead of the relationship between LST and kernels (Gao *et al*., 2006; Xia *et al*., 2019). Among various fusion models (Acronyms are summarized in Table 1), the most widely used technique for LST downscaling is the spatial and temporal adaptive reflectance fusion model (STARFM).

STARFM was originally developed by Gao *et al*. (2006) to downscale daily MODIS surface reflectance to Landsat 30 m resolution. Since then, this method has been widely used for the fusion of other types of images such as LST (Liu and Weng, 2018; Wu *et al*., 2015). The STARFM algorithm (Fig. 3) is summarized as the following equation (3):

$$L(x_{\frac{w}{2}}, y_{\frac{w}{2}}, t_0) = \sum_{i=1}^{w}\sum_{j=1}^{w}\sum_{k=1}^{w}\sum_{ijk} \times (M(x_i, y_j, t_0) + L(x_i, y_j, t_k) - M(x_i, y_j, t_k)) \quad (3)$$

where L and M are Landsat and MODIS surface reflectance, respectively, w is the window size searching similar pixels, $(x_{\frac{w}{2}}, y_{\frac{w}{2}})$ is the location of the center focus pixel, (x_i, y_j) is the pixel location of Landsat and MODIS image pair, t_0 is the target date for downscaling, t_k is

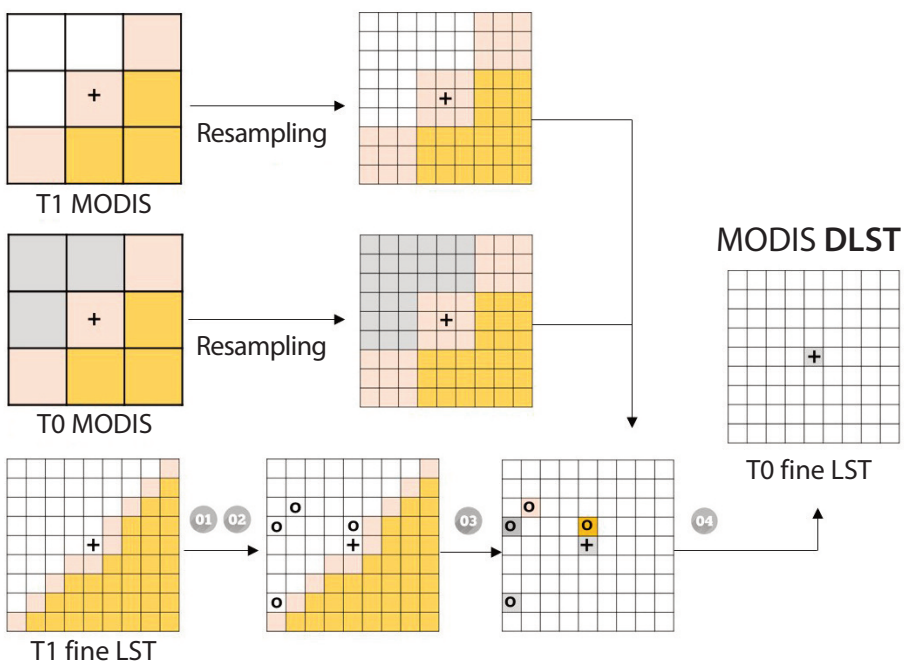

Fig. 3. The flow diagram of spatial and temporal adaptive reflectance fusion model (STARFM) used for MODIS land surface temperature (LST) downscaling: (1) searching pixels (circles) that are spectrally similar to center focus pixel (cross) within a moving window; (2) filtering the searched pixels for ensuring good quality; (3) determining the weights; and (4) downscaled LST (DLST) is generated using the weighted values. The figure is redrawn from Gao *et al.* (2006).

the acquisition date of MODIS and Landsat pairs, and W_{ijk} is the weight that determines the influence of neighboring pixels to the simulated reflectance of the central focus pixel.

Since STARFM assumes that surface cover types and system errors are constant over time, it may result in high uncertainty for LST over heterogenous and time-variant landscapes (Weng *et al*., 2014). Alternatively, Weng *et al*. (2014) proposed Spatio-temporal Adaptive Data Fusion Algorithm for Temperature mapping (SADFAT) by adding the annual temperature cycle (ATC) of LST and thermal landscape heterogeneity of urban area to equation (3), and produced 120 m MODIS DLST over Los Angeles, USA. The enhanced STARFM (ESTARFM) is an alternative method that considers landscape heterogeneity (Zhu *et al*., 2010). ESTARFM uses a conversion coefficient based on spectral unmixing theory and improves the performance of reflectance change prediction for the heterogenous landscapes. Since Wu *et al*. (2015) showed that ESTARFM performed better than STARFM when producing 90 m MODIS DLST, many studies have used ESTARFM for LST downscaling (Yang *et al*., 2016; Li *et al*., 2016; Liu *et al*., 2020b). Recently, Wang *et al*. (2020a) introduced a thermal unmixing based LST downscaling approach using thermal components extracted from Landsat 8 band 4 (0.64-0.67 μm), band 5 (0.85-0.88 μm) and band 10 (10.60-11.19 μm). Yin *et al*. (2020) proposed a deep learning-based spatiotemporal temperature fusion network (STTFN), which fuses images based on convolutional neural networks (CNN) handling the non-linearity of LST temporal changes while the existing fusion-based methods use linear models. In their study, STTFN produced better performance (RMSEs of 1.40 and 1.28K for two study sites) than ESTARFM (RMSEs of 1.90 and 1.49K).

3) Combination of kernel-driven and fusion-based methods

Each of the kernel-driven and fusion-based methods has its own advantages and limitations mentioned in the previous sections. Researchers have put an effort to combine both methods focusing on their advantages (i.e., detailed spatial information from kernels and the capturing ability of the temporal relationship between LST images from fusion). The third type combines the kernel-driven and fusion-based approaches in three ways: 1) kernel-then-fusion (K-F), 2) fusion-then-kernel (F-K), and 3) a weighted combination of kernel and fusion (termed CKFM) (Fig. 4). As an example of K-F, Bai *et al*. (2015) first downscaled Landsat LST to 30 m resolution using Landsat visible, near and shortwave infrared bands as kernels in ELM. Then, they adopted SADFAT to downscale MODIS LST to 30 m DLST. Xia *et al*. (2019) downscaled Landsat LST to 30 m resolution using NDVI and NDBI as kernels in a multivariate function over Beijing, China. They also produced 30 m MODIS LST using STARFM at the same time, and then combined two downscaled LSTs with an inverse error weighted approach (i.e., the

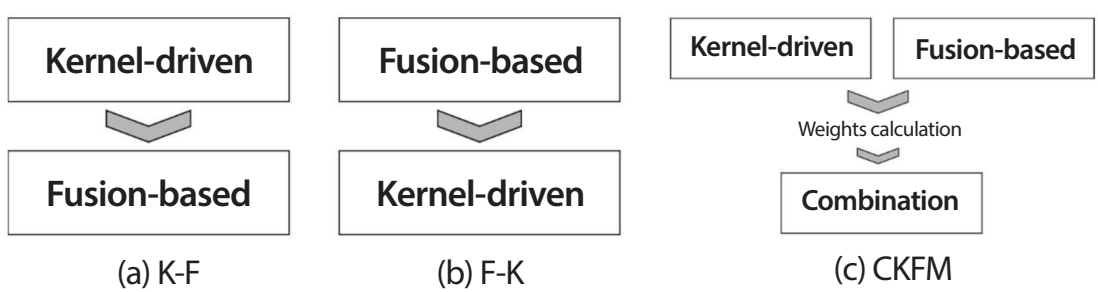

Fig. 4. The three types of combining kernel-driven and fusion-based methods for MODIS LST downscaling.

Table 2. Validation results using Landsat reference LST on October 6, 2014 for the Beijing, China. Adapted from Xia *et al.* (2019)

Methods	Kernel-driven	Fusion-based	Combined kernel-driven and fusion-based		
			K-F	F-K	CKFM
RMSE (K)	1.97	1.53	1.46	1.75	1.39
R	0.66	0.70	0.73	0.69	0.73
MAE (K)	1.50	1.16	1.08	1.31	1.04

larger the error is the smaller the weight). Xia *et al*. (2019) showed that their CKFM model performed better than kernel-driven and fusion-based approaches. They also compared the CKFM model to K-F and F-K, resulting in the higher accuracy of CKFM (Table 2). The proposed CKFM model could compensate for the shortcoming of each of the kernel-driven and fusion-based methods.

3. Open issues and Challenges

Various approaches have been proposed to spatially downscale MODIS LST for the past decade. While their performances have gradually improved, there are still challenges and limitations. Major issues and challenges to discuss here are 1) uncertainty in LST retrievals, 2) low thermal contrast, 3) the nonlinearity of LST temporal change, 4) cloud contamination, and 5) model generalization.

1) Uncertainty in LST Retrievals

There are varied LST retrieval algorithms depending on satellite data used (i.e., MODIS, Landsat, and ASTER). MODIS 1 km LST is retrieved using a generalized split-window (GSW) algorithm based on brightness temperature measured at MODIS band 31 (10.78-11.28 μm) and 32 (11.77-12.27 μm) (equation (4); Wan and Dozier, 1996).

$$LST = b_0 + \left(b_1 + b_2\frac{1-\varepsilon}{\varepsilon} + b_3\frac{\Delta\varepsilon}{\varepsilon^2}\right)\frac{T_{31}+T_{32}}{2} + \left(b_4 + b_5\frac{1-\varepsilon}{\varepsilon} + b_6\frac{\Delta\varepsilon}{\varepsilon^2}\right)\frac{T_{31}-T_{32}}{2} \quad (4)$$

Where ε and Δε refer the mean and difference of the emissivity of band 31 and 32. b_k (K=0 to 6) is the regression coefficient(s) determined in Radiative Transfer Model (RTM) based on the viewing zenith angle, surface air temperature and atmospheric column water vapor. T_{31} and T_{32} are the TIR band brightness temperatures.

Fine resolution ASTER LST is generated based on the temperature emissivity separation (TES) algorithm, which uses a semiempirical relationship between minimum emissivity and the difference between highest and lowest values in the emissivity spectrum (i.e., spectral contrast). The ASTER TES-based algorithm uses an RTM with atmospherically corrected radiance and laboratory measurement-based emissivity to retrieve LST (Gillespie *et al*., 1998). Another fine resolution Landsat sensors, however, do not officially produce LST products until now. One of the widely used LST retrieval algorithms for Landsat data is a single channel (SC) algorithm based on the thermal infrared band (Jiménez-Muñoz *et al*., 2008; Yoo *et al*., 2019). Wu and Li (2019) and Yin *et al*. (2020) discuss that the discrepancy between LST retrieval algorithms by satellite sensor leads to concerns on the accuracy evaluation of LST downscaling.

Furthermore, each LST product has its own retrieval error, which is another challenge for the accurate evaluation of LST downscaling. Major LST retrieval error sources include the lack of understanding for the effects of atmospheric attenuation, insufficient information of the emissivity, and the uncertainties of input factors used for LST retrievals (Ghent *et al*., 2019). The factors required in the MODIS GSW-based

algorithm in equation 4 have their own errors, which increase the uncertainty of MODIS LST.

Although the average error of daytime MODIS LST over homogeneous validation sites was less than RMSE of 1.3K, some stations often resulted in large RMSE > 2K in the literature (Duan *et al*., 2019; Lu *et al*., 2018). Hulley *et al*. (2012) reported that TES-based ASTER LST resulted in an RMSE of 1.2K after water vapor scaling correction. The SC-based algorithm used for Landsat LST extraction is based on radiative transfer equations, requiring thermal path radiance, downwelling irradiance, surface emissivity and the atmospheric transmissivity as input to solve the equations. These factors have generally large variation by spatiotemporal domain, leading to high uncertainty in LST retrieval (Parastatidis *et al*., 2017).

Especially, emissivity is a critical factor in satellite-based LST retrievals. It is well known that small uncertainty in the emissivity (~1%) can result in an LST retrieval error > 1K (Chen *et al*., 2016). While ASTER and MODIS have their own emissivity databases, Landsat lets users directly estimate emissivity to calculate LST. Due to its simplicity, the most widely used method to estimate emissivity is NDVI-based thresholding, which generates several classes by NDVI and applies different emissivity values by class. However, since the NDVI-based emissivity calculation often results in high uncertainty over heterogeneous regions, it is one of the major reasons for the errors that Landsat LST has. In summary, the inherent errors of satellite-based LSTs that are used for training and validation of downscaling make the objective evaluation of LST downscaling difficult.

2) Low Thermal Contrast

The literature shows that downscaled LST has relatively low thermal contrast when compared to high resolution reference LST, which is called blurring effect (Ebrahimy and Azadbakht, 2019; Li *et al*., 2019; Yoo *et al*., 2018; Hutengs and Vohland, 2016). In particular, this problem often occurs when the kernel-driven method with machine learning is used for LST downscaling. Most machine learning approaches tend to estimate output to minimize errors, which are related to the distribution range of training data (Yoo *et al*., 2020). Hutengs and Vohland (2016) showed that RF-based downscaled MODIS LST remarkably blurred with low thermal contrast when compared to reference Landsat LST. Ebrahimy and Azadbakht (2019) reported that machine learning approaches (e.g., RF, SVR) often resulted in better performance than TsHARP, a kernel-driven method, but had relatively larger blurring effect. Li *et al*. (2019) also documented that SVR showed the largest blurring effect among multiple machine learning approaches (i.e., ANN, SVR and RF) for MODIS DLST.

Since machine learning and even deep learning approaches become more popular in LST downscaling due to their powerful performance, minimizing the blurring effect should be one of the core research topics for LST downscaling with machine learning in the future. To reduce the blurring effect, many kernel-driven LST downscaling studies have conducted residual correction that linearly corrects the residuals between 1 km MODIS LST and the aggregation of downscaled LST to 1 km. While the existing studies have typically used global linear regression for residual correction, local or regional correction (e.g., considering land cover characteristics) can be applied to further mitigate the blurring effect. In addition, machine learning can be used to correct the bias that results from a machine learning model for LST downscaling (Song, 2015; Zhang and Lu, 2012).

3) Nonlinearity of LST temporal change

The fusion-based methods have been gradually developed, but there remain issues where typical fusion-based techniques (i.e., STARFM) assume that the output DLST is linearly related to input LSTs. In fact, conventional fusion-based methods assume that the

surface cover type and systemic errors do not change much over time because they were originally suggested for downscaling the reflectance. Unfortunately, while reflectance changes slowly with time, LST has rapid temporal change with nonlinearity (Mohamadi *et al*., 2019). To solve this challenge, some fusion-based studies tried to consider the LST temporal change using the MODIS annual cycle parameters (Weng *et al*., 2014; SADFAT) or thermal components based on the non-negative matrix factorization extracted from the Landsat 8 red, near infrared (NIR) and thermal infrared bands (Wang *et al*., 2020a). Nevertheless, SADFAT could also show the poor downscaling performance over the area with a sudden change in LST (Quan *et al*., 2016).

Recently, a fusion approach of LST images was proposed using the non-linear fitting model, such as a deep learning-based CNN (i.e., STTFN; Yin *et al*., 2020). It should be noted that STTFN is able to build up the complicated relationship without manually designed mathematical rules as the conventional fusion models because it can directly model the nonlinear relationship between the input and output LSTs. However, as the deep learning model relies on the training samples, the developed model has limitations that might not work well over different areas without training. In addition, deep learning approaches often have overfitting problems by optimizing a large number of parameters (Li *et al*., 2018), which should be further examined. Thus, there is still a room for further investigating various up-to-date deep learning-based algorithms to be grafted into LST image fusion for downscaling.

4) Cloud Contamination

Thermal infrared (TIR) sensors such as MODIS, Landsat, and ASTER are the most widely used one to retrieve LSTs. One of the most critical problems when using TIR-derived LSTs is the sensitivity to atmospheric and weather conditions. In particular, global mean cloud cover from 2003 to 2012 is about 66%, where 59.7% over North America and 56.0% over Asia (Mao *et al*., 2019). Unfortunately, LST retrievals from TIR sensors are not available under clouds due to their inability to penetrate clouds (i.e., cloud contamination) (Yoo *et al*., 2020). In addition, the time interval of high resolution LST images such as Landsat and ASTER ones is large (i.e., 16 days), which makes it much difficult to match MODIS LST under the clear-sky condition.

An alternative to reducing the time interval is to estimate satellite-based LST under the cloudy condition before conducting LST downscaling. Brightness temperature of passive microwave (PMW) data, known to have high correlation with LST, can be used to estimate LST for cloudy MODIS pixels (Fu *et al*., 2019; Yoo *et al*., 2020). However, it is still challenging to accurately estimate LST for cloudy MODIS pixels mainly due to the low spatial resolution of PMW (e.g., 10 km). Future PMW sensors with higher spatial resolution may improve LST estimation under cloudy pixels. The high temporal resolution of geostationary satellite instruments, such as GK-2A AMI LSTs could assist for identifying the diurnal cycle of LST and the temporal variation of cloud covers. For example, Zhao and Duan (2020) proposed a method to reconstruct MODIS daytime LST under cloud areas based on the solar radiation factor (i.e., cumulative downward shortwave radiation flux) calculated from geostationary SEVIRI LST.

5) Model Generalization

Most LST downscaling methods developed for the past decade have been evaluated over local areas, which limits the generalization of the proposed methods. The performance of the methods often varied by the characteristics of climate and land cover types (Yang *et al*., 2017; Wang *et al*., 2020a). For example, the methods using NDVI or EVI as kernels (i.e., DisTrad, TsHARP) might not work well for areas with low correlation between vegetation indices and LST

(Mukherjee *et al*., 2014; Qiu *et al*., 2018). One possible solution to ensure LST downscaling approaches to have a generalized capability is to evaluate them over multiple areas with different conditions and optimize the related parameters. It should be noted that only a small number of studies among those reviewed in this paper have more than one study area for MODIS LST downscaling (Peng *et al*., 2019; Wu *et al*., 2019; Liu *et al*., 2019; Wang *et al*., 2020a; Yin *et al*., 2020). Moreover, most LST downscaling studies used high resolution LST data as reference and did not use in situ LST measurements. Of course, there exists the scale discrepancy between satellite observations and in situ measurements. Nonetheless, given that in situ data are the most accurate LST measurements and satellite-derived LST has uncertainty, it is crucial to incorporate in situ measurements to evaluate LST downscaling models.

4. Future research directions

Based on the comprehensive review of the MODIS LST downscaling studies published during the past 10 years, the future research directions of thermal downscaling can be drawn as follows.

Using various data types to produce DLST with very high spatial resolution: In the field of urban planning and management, very high resolution (< 10 m) LST or DLST becomes more important in order to examine the dynamics of thermal phenomena such as urban heat island effect over heterogeneous urban areas. The detailed LST or DLST can identify fine scale urban features such as buildings and green spaces (Hulley *et al*., 2019). For example, since Sentinel 2 reflectance (10 m resolution red, green, blue and NIR bands) has higher spatiotemporal resolution than Landsat (30 m resolution red, green, blue and NIR bands), it can be used as kernels to generate high resolution DLST (e.g., at 10 m). Recently, in order to reduce the cost and time for satellite development, the constellation of small and micro satellites with very high resolution and quick revisit (e.g., PlanetScope and SkySat) have been launched. In the future, data from the satellite constellation can be used for LST downscaling to improve the spatiotemporal resolution of DLST. Another way to produce very high resolution LST (or DLST) is to fuse satellite observations with numerical models at fine resolution (e.g., 1-10 m). For example, the computational fluid dynamics (CFD) model, one of the numerical models for simulating local atmospheric dynamics, can produce high resolution atmospheric parameters such as wind, air temperature, and net radiation using detailed topography and building information (Kim *et al*., 2017). Such a model can be combined with satellite data for LST downscaling, which can be used to monitor complicated thermal characteristics in urban areas at street level.

Reducing the uncertainty of LST products: There are many factors that influence the quality of DLST, including the quality of LST and input variables, and cloud contamination. Generally, when coarse resolution LST has high quality on the spatiotemporal domains, there is high chance for DLST to have high quality as well. Thus, efforts to minimize LST retrieval errors and to standardize the LST retrieval processes can improve the quality of DLST in the future. For example, TES-based MODIS LST (i.e., MYD21 products) has recently been provided. As the TES-based LST is known to have low LST retrieval error over hot and humid regions due to its improved water vapor scaling atmospheric correction (Hulley *et al*., 2016b), LST downscaling of MYD21 with ASTER LST that uses the same retrieval algorithm can improve the performance. The use of high spatial resolution LST data with high temporal resolution can mitigate the cloud contamination problem for LST downscaling. For example, the recently launched Ecostress has the spatial resolution of 70 m and the temporal resolution of 3-5 days, which are much better for LST downscaling when compared to

Landsat and ASTER LST data as input (Hulley *et al*., 2019).

Using state-of-the-art models such as deep learning: While many studies have used various statistical models for MODIS LST downscaling, a few have utilized deep learning approaches. While CNN has been used in the image fusion-based method for LST downscaling (Yin *et al*., 2020), performance could be further improved if additional input data such as *in-situ* LST or other numerical model data were used together. Recently, several studies showed that advanced deep-learning model—generative adversarial network (GAN)—improved the image pan-sharpening performance than CNN (Liu *et al*., 2018; Zhang *et al*., 2020). Therefore, GAN using adversarial supervision between generator and discriminator, or other types of up-to-date deep learning approaches can be used for LST downscaling to produce more reliable DLST in the future.

Increasing model generalization: One of the major problems of the existing LST downscaling studies is their locality. Considering that high resolution LST is often necessary at regional or global scale, it is crucial to use the downscaling methods that can be generalized. Thus, future LST downscaling research should focus on the generalization of the methods under investigation over various study sites with different land cover characteristics. Comprehensive evaluation using in situ measurements or cross-site validation should follow to ensure the model generalization.

Using geostationary satellite-derived LSTs: While most MODIS LST downscaling studies have used polar-orbiting satellite data such as Landsat and ASTER. With the increasing interest in the diurnal cycle of LST over urban areas (Yamamoto and Ishikawa, 2018), geostationary satellite-derived LST with relatively coarse resolution can be used for LST downscaling along with high resolution satellite data. Geostationary satellite LST can be used as LST image pairs along with MODIS and Landsat incorporated in a fusion-based method. In particular, a method of spatio-temporal reconstruction of a geostationary satellite-based LST has been proposed in various ways, from using a diurnal cycle curve (Liu *et al*., 2017) to a method using CNN (Wu *et al*., 2019). When geostationary satellite data are used in LST downscaling, the temporal resolution of the DLST can be significantly improved. It is also expected that a relatively seamless output can be produced through temporal interpolation (i.e., using the diurnal cycle of LST) over cloud contaminated areas.

5. Conclusion

The present paper reviewed the MODIS LST downscaling studies published for the past 10 years. The three types of approaches—kernel-driven, fusion-based, and the combination of the first two—were used to downscale MODIS LST (1 km) to higher spatial scales (e.g., 30 m, 90 m). However, although many studies have been conducted on thermal downscaling, several limitations mentioned in the previous section still remain in terms of input data, methods, and validation. Five future research directions of thermal downscaling discussed in section 4 will guide scientists to effectively mitigate the challenges to increase the contribution of DLST to various research fields.

Acknowledgements

This research was supported by the Institute for Information & communications Technology Promotion (IITP) supported by the Ministry of Science and ICT (MSIT), Korea (IITP-2020-2018-0-01424), and the Korea Meteorological Administration Research and Development Program under grant KMIPA 2017-7010. CY was also supported by Global PhD Fellowship Program through the National Research Foundation of

Korea (NRF), funded by the Ministry of Education (NRF-2018H1A2A1062207).

References

Abrams, M., S. Hook, and B. Ramachandran, 2002. ASTER user handbook, https://asterweb.jpl.nasa.gov, Accessed on Aug. 20, 2020.

Agathangelidis, I. and C. Cartalis, 2019. Improving the disaggregation of MODIS land surface temperatures in an urban environment: a statistical downscaling approach using high-resolution emissivity, *International Journal of Remote Sensing*, 40(13): 5261-5286.

Albright, T. P., A. M. Pidgeon, C. D. Rittenhouse, M. K. Clayton, C. H. Flather, P. D. Culbert, and V. C. Radeloff, 2011. Heat waves measured with MODIS land surface temperature data predict changes in avian community structure, *Remote Sensing of Environment*, 115(1): 245-254.

Alkhaier, F., G. Flerchinger, and Z. Su, 2012. Shallow groundwater effect on land surface temperature and surface energy balance under bare soil conditions: modeling and description, *Hydrology and Earth System Science*s, 16(7): 1817.

Atitar, M., J. A. Sobrino, G. Soria, J.-P. Wigneron, J. C. Jiménez-Muñoz, Y. Julien, and A. B. Ruescas, 2008. Land surface temperature retrieved from SEVIRI/MSG2 data: algorithm and validation, *Proc. of EUMETSAT Meteorological Satellite Conference*, Darmstadt, Germany, Sep. 8-12, pp. 1-5.

Bai, Y., M. S. Wong, W.-Z. Shi, L.-X. Wu, and K. Qin, 2015. Advancing of land surface temperature retrieval using extreme learning machine and spatio-temporal adaptive data fusion algorithm, *Remote Sensing*, 7(4): 4424-4441.

Bartkowiak, P., M. Castelli, and C. Notarnicola, 2019. Downscaling land surface temperature from MODIS dataset with random forest approach over alpine vegetated areas, *Remote Sensing*, 11(11): 1319.

Bateni, S., D. Entekhabi, and D.-S. Jeng, 2013. Variational assimilation of land surface temperature and the estimation of surface energy balance components, *Journal of Hydrology*, 481: 143-156.

Bonafoni, S., 2016. Downscaling of Landsat and MODIS land surface temperature over the heterogeneous urban area of Milan, *IEEE Journal of Selected Topics in Applied Earth Observations and Remote Sensing*, 9(5): 2019-2027.

Chen, F., S. Yang, Z. Su, and K. Wang, 2016. Effect of emissivity uncertainty on surface temperature retrieval over urban areas: Investigations based on spectral libraries, *ISPRS Journal of Photogrammetry and Remote Sensing*, 114: 53-65.

Duan, S.-B., X.-J. Han, C. Huang, Z.-L. Li, H. Wu, Y. Qian, M. Gao, and P. Leng, 2020. Land Surface Temperature Retrieval from Passive Microwave Satellite Observations: State-of-the-Art and Future Directions, *Remote Sensing*, 12(16): 2573.

Duan, S.-B. and Z.-L. Li, 2016. Spatial downscaling of MODIS land surface temperatures using geographically weighted regression: Case study in northern China, *IEEE Transactions on Geoscience and Remote Sensing*, 54(11): 6458-6469.

Duan, S.-B., Z.-L. Li, H. Li, F.-M. Göttsche, H. Wu, W. Zhao, P. Leng, X. Zhang, and C. Coll, 2019. Validation of Collection 6 MODIS land surface temperature product using in situ measurements, *Remote Sensing of Environment*, 225: 16-29.

Ebrahimy, H. and M. Azadbakht, 2019. Downscaling MODIS land surface temperature over a

heterogeneous area: An investigation of machine learning techniques, feature selection, and impacts of mixed pixels, *Computers & Geosciences*, 124: 93-102.

Fu, P., Y. Xie, Q. Weng, S. Myint, K. Meacham-Hensold, and C. Bernacchi, 2019. A physical model-based method for retrieving urban land surface temperatures under cloudy conditions, *Remote Sensing of Environment*, 230: 111191.

Gao, F., J. Masek, M. Schwaller, and F. Hall, 2006. On the blending of the Landsat and MODIS surface reflectance: Predicting daily Landsat surface reflectance, *IEEE Transactions on Geoscience and Remote Sensing*, 44(8): 2207-2218.

Ghent, D., K. Veal, T. Trent, E. Dodd, H. Sembhi, and J. Remedios, 2019. A new approach to defining uncertainties for MODIS land surface temperature, *Remote Sensing*, 11(9): 1021.

Gillespie, A., S. Rokugawa, T. Matsunaga, J. S. Cothern, S. Hook, and A. B. Kahle, 1998. A temperature and emissivity separation algorithm for Advanced Spaceborne Thermal Emission and Reflection Radiometer (ASTER) images, *IEEE Transactions on Geoscience and Remote Sensing*, 36(4): 1113-1126.

Hain, C. R. and M. C. Anderson, 2017. Estimating morning change in land surface temperature from MODIS day/night observations: Applications for surface energy balance modeling, *Geophysical Research Letters*, 44(19): 9723-9733.

Hulley, G., T. Islam, R. Freepartner, and N. Malakar, 2016a. *Visible Infrared Imaging Radiometer Suite (VIIRS) Land Surface Temperature and Emissivity Product Collection 1 Algorithm Theoretical Basis Document*, Jet Propulsion Laboratory, Pasadena, CA, USA.

Hulley, G., N. Malakar, and R. Freepartner, 2016b. *Moderate Resolution Imaging Spectroradiometer (MODIS) Land Surface Temperature and Emissivity Product (MxD21) Algorithm Theoretical Basis Document Collection-6*, JPL Publication, Pasadena, CA, USA, pp. 12-17.

Hulley, G., S. Shivers, E. Wetherley, and R. Cudd, 2019. New ECOSTRESS and MODIS land surface temperature data reveal fine-scale heat vulnerability in cities: A case study for Los Angeles County, California, *Remote Sensing*, 11(18): 2136.

Hulley, G. C., C. G. Hughes, and S. J. Hook, 2012. Quantifying uncertainties in land surface temperature and emissivity retrievals from ASTER and MODIS thermal infrared data, *Journal of Geophysical Research: Atmospheres*, 117: D23.

Hutengs, C. and M. Vohland, 2016. Downscaling land surface temperatures at regional scales with random forest regression, *Remote Sensing of Environment*, 178: 127-141.

Jiménez-Muñoz, J. C., J. Cristóbal, J. A. Sobrino, G. Sòria, M. Ninyerola, and X. Pons, 2008. Revision of the single-channel algorithm for land surface temperature retrieval from Landsat thermal-infrared data, *IEEE Transactions on Geoscience and Remote Sensing*, 47(1): 339-349.

Kim, D.-H., G.-H. Kim, J.-Y. Byon, B.-J. Kim, and J.-J. Kim, 2017. The Verification of a Numerical Simulation of Urban area Flow and Thermal Environment Using Computational Fluid Dynamics Model, *Journal of the Korean Earth Science Society*, 38(7): 522-534.

Kustas, W. P., J. M. Norman, M. C. Anderson, and A. N. French, 2003. Estimating subpixel surface temperatures and energy fluxes from the vegetation index-radiometric temperature relationship, *Remote Sensing of Environment*, 85(4): 429-440.

Li, Q., F. Ding, W. Wu, and J. Chen, 2016. Improvement of ESTARFM and its application to fusion of Landsat-8 and MODIS land surface temperature images, *Proc. of 4th International*

Workshop on Earth Observation and Remote Sensing Applications (EORSA), Guangzhou, China, pp. 33-37.

Li, W., L. Ni, Z.-L. Li, S.-B. Duan, and H. Wu, 2019. Evaluation of machine learning algorithms in spatial downscaling of MODIS land surface temperature, *IEEE Journal of Selected Topics in Applied Earth Observations and Remote Sensing*, 12(7): 2299-2307.

Li, Y., H. Zhang, X. Xue, Y. Jiang, and Q. Shen, 2018. Deep learning for remote sensing image classification: A survey, *Wiley Interdisciplinary Reviews: Data Mining and Knowledge Discovery*, 8(6): e1264.

Liu, H. and Q. Weng, 2018. Scaling effect of fused ASTER-MODIS land surface temperature in an urban environment, *Sensors*, 18(11): 4058.

Liu, K., S. Wang, X. Li, Y. Li, B. Zhang, and R. Zhai, 2020a. The assessment of different vegetation indices for spatial disaggregating of thermal imagery over the humid agricultural region, *International Journal of Remote Sensing*, 41(5): 1907-1926.

Liu, K., S. Wang, X. Li, and T. Wu, 2019. Spatially Disaggregating Satellite Land Surface Temperature With a Nonlinear Model Across Agricultural Areas, *Journal of Geophysical Research: Biogeosciences*, 124(11): 3232-3251.

Liu, X., Y. Wang, and Q. Liu, 2018. PSGAN: A generative adversarial network for remote sensing image pan-sharpening, *Proc. of 25th IEEE International Conference on Image Processing (ICIP)*, Athens, Greece, Oct. 7-10, pp. 873-877.

Liu, X., Y. Zhou, W. Yue, X. Li, Y. Liu, and D. Lu, 2020b. Spatiotemporal patterns of summer urban heat island in Beijing, China using an improved land surface temperature, *Journal of Cleaner Production*, 257: 120529.

Liu, Z., P. Wu, S. Duan, W. Zhan, X. Ma, and Y. Wu, 2017. Spatiotemporal reconstruction of land surface temperature derived from fengyun geostationary satellite data, *IEEE Journal of Selected Topics in Applied Earth Observations and Remote Sensing*, 10(10): 4531-4543.

Lu, L., T. Zhang, T. Wang, and X. Zhou, 2018. Evaluation of collection-6 MODIS land surface temperature product using multi-year ground measurements in an arid area of Northwest China, *Remote Sensing*, 10(11): 1852.

Maeda, E. E., 2014. Downscaling MODIS LST in the East African mountains using elevation gradient and land-cover information, *International Journal of Remote Sensing*, 35(9): 3094-3108.

Mao, K., Z. Yuan, Z. Zuo, T. Xu, X. Shen, and C. Gao, 2019. Changes in global cloud cover based on remote sensing data from 2003 to 2012, *Chinese Geographical Science*, 29(2): 306-315.

Meng, C., Z. L. Li, X. Zhan, J. Shi, and C. Liu, 2009. Land surface temperature data assimilation and its impact on evapotranspiration estimates from the Common Land Model, *Water Resources Research*, 45(2): W02421.

Mohamadi, B., S. Chen, T. Balz, K. Gulshad, and S. C. McClure, 2019. Normalized Method for Land Surface Temperature Monitoring on Coastal Reclaimed Areas, *Sensors*, 19(22): 4836.

Mukherjee, S., P. Joshi, and R. Garg, 2014. A comparison of different regression models for downscaling Landsat and MODIS land surface temperature images over heterogeneous landscape, *Advances in Space Research*, 54(4): 655-669.

Pan, X., X. Zhu, Y. Yang, C. Cao, X. Zhang, and L. Shan, 2018. Applicability of downscaling land surface temperature by using normalized difference sand index, *Scientific Reports*, 8(1): 1-14.

Parastatidis, D., Z. Mitraka, N. Chrysoulakis, and M. Abrams, 2017. Online global land surface temperature estimation from Landsat, *Remote*

Sensing, 9(12): 1208.

Park, S., D. Kang, C. Yoo, J. Im, and M.-I. Lee, 2020. Recent ENSO influence on East African drought during rainy seasons through the synergistic use of satellite and reanalysis data, *ISPRS Journal of Photogrammetry and Remote Sensing*, 162: 17-26.

Peng, Y., W. Li, X. Luo, and H. Li, 2019. A geographically and temporally weighted regression model for spatial downscaling of MODIS land surface temperatures over urban heterogeneous regions, *IEEE Transactions on Geoscience and Remote Sensing*, 57(7): 5012-5027.

Qiu, J., J. Yang, Y. Wang, and H. Su, 2018. A comparison of NDVI and EVI in the DisTrad model for thermal sub-pixel mapping in densely vegetated areas: A case study in Southern China, *International Journal of Remote Sensing*, 39(8): 2105-2118.

Quan, J., W. Zhan, Y. Chen, M. Wang, and J. Wang, 2016. Time series decomposition of remotely sensed land surface temperature and investigation of trends and seasonal variations in surface urban heat islands, *Journal of Geophysical Research: Atmospheres*, 121(6): 2638-2657.

Sánchez, J. M., J. M. Galve, J. González-Piqueras, R. López-Urrea, R. Niclòs, and A. Calera, 2020. Monitoring 10-m LST from the Combination MODIS/Sentinel-2, Validation in a High Contrast Semi-Arid Agroecosystem, *Remote Sensing*, 12(9): 1453.

Sattari, F., M. Hashim, and A. B. Pour, 2018. Thermal sharpening of land surface temperature maps based on the impervious surface index with the TsHARP method to ASTER satellite data: A case study from the metropolitan Kuala Lumpur, Malaysia, *Measurement*, 125: 262-278.

Song, J., 2015. Bias corrections for random forest in regression using residual rotation, *Journal of the Korean Statistical Society*, 44: 321-326.

Srivastava, P. K., D. Han, M. R. Ramirez, and T. Islam, 2013. Machine learning techniques for downscaling SMOS satellite soil moisture using MODIS land surface temperature for hydrological application, *Water Resources Management*, 27(8): 3127-3144.

USGS, 2016. Landsat 8 (L8) data users handbook, Department of the Interior US Geological Survey, https://www.usgs.gov/land-resources/nli/landsat/landsat-8-data-users-handbook, Accessed on Aug. 20, 2020.

Wan, Z., 1999. *MODIS land-surface temperature algorithm theoretical basis document (LST ATBD)*, Institute for Computational Earth System Science, Santa Barbara, CA, USA, p. 75.

Wan, Z. and J. Dozier, 1996. A generalized split-window algorithm for retrieving land-surface temperature from space, *IEEE Transactions on Geoscience and Remote Sensing*, 34(4): 892-905.

Wang, J., O. Schmitz, M. Lu, and D. Karssenberg, 2020a. Thermal unmixing based downscaling for fine resolution diurnal land surface temperature analysis, *ISPRS Journal of Photogrammetry and Remote Sensing*, 161: 76-89.

Wang, R., W. Gao, and W. Peng, 2020b. Downscale MODIS Land Surface Temperature Based on Three Different Models to Analyze Surface Urban Heat Island: A Case Study of Hangzhou, *Remote Sensing*, 12(13): 2134.

Weng, Q., P. Fu, and F. Gao, 2014. Generating daily land surface temperature at Landsat resolution by fusing Landsat and MODIS data, *Remote Sensing of Environment*, 145: 55-67.

Wu, H. and W. Li, 2019. Downscaling land surface temperatures using a random forest regression model with multitype predictor variables, *IEEE Access*, 7: 21904-21916.

Wu, M., H. Li, W. Huang, Z. Niu, and C. Wang, 2015.

Generating daily high spatial land surface temperatures by combining ASTER and MODIS land surface temperature products for environmental process monitoring, *Environmental Science: Processes & Impacts*, 17(8): 1396-1404.

Wu, P., Z. Yin, H. Yang, Y. Wu, and X. Ma, 2019. Reconstructing geostationary satellite land surface temperature imagery based on a multiscale feature connected convolutional neural network, *Remote Sensing*, 11(3): 300.

Xia, H., Y. Chen, Y. Li, and J. Quan, 2019. Combining kernel-driven and fusion-based methods to generate daily high-spatial-resolution land surface temperatures, *Remote Sensing of Environment*, 224: 259-274.

Yamamoto, Y. and H. Ishikawa, 2018. Spatiotemporal variability characteristics of clear-sky land surface temperature in urban areas of Japan observed by Himawari-8, *Sola*, 14: 179-184.

Yamamoto, Y., H. Ishikawa, Y. Oku, and Z. Hu, 2018. An algorithm for land surface temperature retrieval using three thermal infrared bands of Himawari-8, *Journal of the Meteorological Society of Japan*, 96B: 43-58.

Yang, G., Q. Weng, R. Pu, F. Gao, C. Sun, H. Li, and C. Zhao, 2016. Evaluation of ASTER-like daily land surface temperature by fusing ASTER and MODIS data during the HiWATER-MUSOEXE, *Remote Sensing*, 8(1): 75.

Yang, Y., C. Cao, X. Pan, X. Li, and X. Zhu, 2017. Downscaling land surface temperature in an arid area by using multiple remote sensing indices with random forest regression, *Remote Sensing*, 9(8): 789.

Yin, Z., P. Wu, G. M. Foody, Y. Wu, Z. Liu, Y. Du, and F. Ling, 2020. Spatiotemporal Fusion of Land Surface Temperature Based on a Convolutional Neural Network, https://ieeexplore.ieee.org/document/9115890, Accessed on Aug. 17, 2020.

Yoo, C., J. Im, D. Cho, N. Yokoya, J. Xia, and B. Bechtel, 2020. Estimation of All-Weather 1 km MODIS Land Surface Temperature for Humid Summer Days, *Remote Sensing*, 12(9): 1398.

Yoo, C., J. Im, S. Park, and D. Cho, 2017. Thermal characteristics of Daegu using land cover data and satellite-derived surface temperature downscaled based on machine learning, *Korean Journal of Remote Sensing*, 33(6-2): 1101-1118 (in Korean with English abstract).

Yoo, C., J. Im, S. Park, and L. J. Quackenbush, 2018. Estimation of daily maximum and minimum air temperatures in urban landscapes using MODIS time series satellite data, *ISPRS Journal of Photogrammetry and Remote Sensing*, 137: 149-162.

Yoo, C., S. Park, Y. Kim, and D. Cho, 2019. Analysis of Thermal Environment by Urban Expansion using KOMPSAT and Landsat 8: Sejong City, *Korean Journal of Remote Sensing*, 35(6-4): 1403-1415 (in Korean with English abstract).

Yu, Y., D. Tarpley, H. Xu, and M. Chen, 2010. *Goes-r advanced baseline imager (abi) algorithm theoretical basis document for land surface temperature*, NOAA NESDIS Center for Satellite Applications and Research, Camp Springs, MD, USA.

Zhang, G. and Y. Lu, 2012. Bias-corrected random forests in regression, *Journal of Applied Statistics*, 39(1): 151-160.

Zhang, H., Y. Song, C. Han, and L. Zhang, 2020. Remote Sensing Image Spatiotemporal Fusion Using a Generative Adversarial Network, https://ieeexplore.ieee.org/abstract/document/9159647, Accessed on Aug. 18, 2020.

Zhao, W. and S.-B. Duan, 2020. Reconstruction of daytime land surface temperatures under cloud-covered conditions using integrated MODIS/Terra land products and MSG geostationary satellite data, *Remote Sensing of Environment*, 247: 111931.

Zhu, X., J. Chen, F. Gao, X. Chen, and J. G. Masek, 2010. An enhanced spatial and temporal adaptive reflectance fusion model for complex heterogeneous regions, *Remote Sensing of Environment*, 114(11): 2610-2623.

Ziaul, S. and S. Pal, 2018. Analyzing control of respiratory particulate matter on Land Surface Temperature in local climatic zones of English Bazar Municipality and Surroundings, *Urban Climate*, 24: 34-50.